Epoxy Reinforced Aerogels Made Using a Streamlined Process

Mary Ann B. Meador,* Christopher M. Scherzer,[†] Stephanie L. Vivod, Derek Quade, and Baochau N. Nguyen[‡]

NASA Glenn Research Center, 21000 Brookpark Road, Cleveland, Ohio 44135

ABSTRACT Reinforcing silica aerogels by conformally coating the nanoskeleton with a polymer has been demonstrated to be an effective way to improve mechanical properties. In addition, the mesoporosity and low thermal conductivity is maintained, making this robust form of aerogel an enabling material for a variety of aerospace applications. However, the process for making the aerogels can be quite long, involving production of the gel, solvent exchanges, and diffusion of monomer, followed by more solvent washes and supercritical fluid extraction. This paper for the first time compares a synthetic scheme that shortens the process to make epoxy reinforced aerogels by eliminating monomer diffusion and half of the solvent washes to the previously described diffusion-controlled process. The ethanol-soluble epoxy monomers are included in the initial step of the sol–gel process without interfering with gelation of the starting silanes. Notably, properties of aerogels made using a low amount of amine reactive sites have properties similar to those previously reported that used the longer diffusion controlled process, whereas higher amounts of amine sites produce less desirable monoliths with much higher density and lower surface areas.

KEYWORDS: aerogels • polymer cross-linking • nanoporous materials • hybrid materials • sol–gel

INTRODUCTION

Light weight and low thermal conductivity make aerogels an enabling material for a variety of aerospace and other applications (1). Durable aerogels are especially important as insulation for habitats, space suits, and other astronaut equipment for future Mars surface missions. Multilayer insulation (MLI), used for insulation in extravehicular activity (EVA) suits for space or the moon and comprising many thin layers of polymer such as Kapton or Mylar metalized on one side with aluminum or silver, requires a high vacuum to be effective. In evacuated conditions, contact points between the separate layers in MLI are reduced. Hence, conduction and convection are minimized. The multiple layers reduce the last form of heat transfer, radiation, by radiating and absorbing heat from each other, effectively trapping most of the thermal energy. Because the atmospheric surface pressure on Mars averages around 6 Torr, MLI is not suitable as insulation (2). Of a variety of materials considered in a recent study, only aerogel fiber composites were found to be effective candidates for Mars surface suit insulation (3), although they tended to shed silica particles at unacceptable levels (4).

Reinforcing silica aerogels using a conformal coating of di-isocyanate on the silica nanoskeleton has been demonstrated to be an effective way to improve mechanical properties and possibly reduce shedding (5). Introducing reactive sites to the silica surface improves the cross-linking with di-isocyanate (6) and allows a variety of monomers to be used for reinforcement, including cyanoacrylates (7), styrene (8), and epoxy (9). Epoxy reinforced aerogels, as shown in Scheme 1, are especially interesting because we have recently demonstrated that these can be produced using ethanol instead of more expensive, less environmentally friendly solvents employed with other cross-linkers (10). Because so much solvent is used in the process of making the aerogels, this has a considerable effect on the cost to produce the aerogels. However, as seen in Scheme 2, the multistep process for making polymer reinforced aerogels can be quite long, involving production of the gel, solvent exchanges, diffusion of monomer, and heating to react the monomer, followed by more solvent exchanges and supercritical fluid extraction (SFE). This paper discusses a new synthetic scheme that shortens the process to make epoxy reinforced aerogels by eliminating monomer diffusion and at least half of the solvent washes. In this one-pot process, the ethanol soluble epoxy monomer is included in the initial step of the sol–gel process. A similar scheme was recently used to produce aerogels cross-linked with polyacrylonitrile (PAN) (11). Analogous to this example, and unlike other previous cross-linking chemistry, it will be shown that monomer incorporation does not interfere with gelation of the silane precursors. In addition, the effects of four different variables on the properties of the resulting aerogels made using the new one-pot method are discussed and compared to previously reported aerogels using the multistep, diffusion controlled process (10). In this way, we show for the first time the fundamental differences between aerogels made using the two processes. Variables shown in Table 1 include total Si concentration, fraction of the total Si derived from bis(trimethoxysilyl)hexane (BTMSH) and 3-aminopropyltriethoxysilane (APTES), the concentration of epoxy monomer

Scheme 1. Typical Reaction Scheme for Cross-Linking Silica Gels with Epoxy through Surface Amine Groups

R =

BPGE
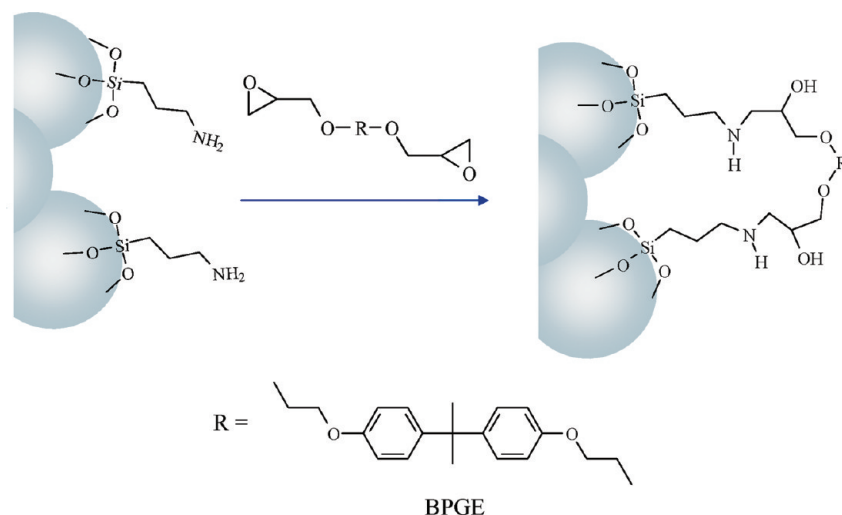
Scheme 2. Comparison of One Pot with Multistep Diffusion Process for Fabricating Epoxy Reinforced Aerogels
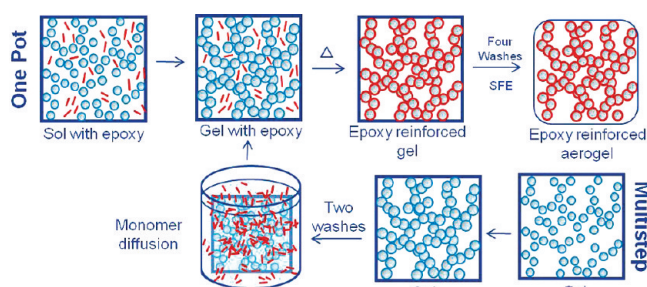
in the initial sol and the method used to control gelation. APTES provides amines on the silica gel surface for reaction with epoxy, whereas the hexyl links from BTMSH have been shown to improve flexibility of the underlying silica backbone, resulting in less brittle failure (10).

EXPERIMENTAL SECTION

Reagents. Tetraethylorthosilicate (TEOS), 1,6-bis(trimethoxysilyl)hexane (BTMSH), and 3-aminopropyl-triethoxysilane (APTES) were purchased from Gelest, Inc. Bisphenol-A propoxylate diglycidyl ether (BPGE) was purchased from Aldrich Chemical Co. Ethanol (100%) was purchased from Pharmco Products, Inc. All reagents were used without further purification.

General. Supercritical fluid extraction was carried out with an Applied Separations 1 L SPE-ED SFE-2. Solid ^{29}Si and ^{13}C NMR spectra of the aerogels were obtained on a Bruker Avance 300 spectrometer using 4 mm solids probe with cross-polarization and magic angle spinning at 11 kHz. ^{13}C spectra were externally referenced to the carbonyl of glycine which appears at 176.1 ppm relative to tetramethylsilane (TMS). ^{29}Si spectra were externally referenced to 3-trimethoxysilylpropionic acid at 0 ppm. Samples for microscopy were coated with gold/palladium and viewed using a Hitachi S-4700−11 field emission scanning electron microscope. Skeletal densities of the aerogels were obtained on a Micromeritics Accupyc 1340 Helium Pycnometer. Nitrogen sorption porosimetry was carried out on an ASAP 2000 surface area/pore size distribution analyzer (Micromeritics Instrument Corp.). Samples were outgassed by heating at 60 °C under a vacuum for 8 h prior to testing.

Process of Making Aerogels. TEOS derived gels were made using a modified two-step process involving acid hydrolysis of TEOS, followed by base catalyzed condensation with APTES (and BTMSH if used). To illustrate, a typical procedure is outlined for a formulation with total Si concentration of 1.6 mol/L of the total sol, APTES Si fraction of 15 mol % and epoxy monomer, BPGE, in a 0.5 to 1 ratio to APTES (run 2 in Table 1). To a solution of 30.3 mL of TEOS (0.136 mol) in 16.3 mL of ethanol was added a solution of 14.4 mL of water (0.8 mols, based on a 5 to 1 ratio of water to total Si) and 0.005 mL concentrated nitric acid in 14.4 mL ethanol with stirring. The combined solution was stirred for 1 h. In the meantime, another solution was prepared consisting of 5.6 mL APTES (0.024 mol) and epoxy monomer, BPGE, (5.48 g, 0.012 mol) in 14.4 mL ethanol. These two solutions were cooled in a dry ice−acetone bath before combining and shaking vigorously. The resulting 100 mL of solution was then poured into five cylindrical molds, nominally 20 mm in diameter, which were made by cutting the needle end off of Norm-ject syringes and extending the plunger nearly all the way out. The gels, which formed in 5 to 15 min, were aged for 24 h before being extracted into clean ethanol by being pushed out of the molds with the plunger. The samples were heated for 24 h in a 70 °C oven to react the epoxy with amine. After cooling and four solvent exchanges, the gels were dried by supercritical CO_2 fluid extraction followed by vacuum drying, yielding monoliths with average density of 0.365 g/cm^3.

Compression Tests. A cylindrical specimen from each run was sectioned in half with a scroll saw. The top and bottom of each specimen was sanded and checked using an L-square to make certain that these surfaces were smooth and parallel. The samples were tested between a pair of compression platens on a Model 4505 Instron load frame using the Series IX data acquisition software. The platen surfaces were coated with a graphite lubricant to reduce the surface friction and barreling of the specimen. The specimens were tested in accordance with ASTM D695 with the exception of sample size. Although the ASTM standard calls for a slenderness ratio of 11−16 to 1, typified by a cylinder 12.7 mm in diameter by 50.8 mm in length, using this sample size in our testing lead to buckling in lower density specimens. In this study, the samples are nominally 16−18 mm in diameter and about 25−30 mm in length with a slenderness ratio of about 6−7 to 1.

Load−unload tests were also performed to determine the extent to which the samples recover after compression. In this case, samples were prepared identically to those for straight compression and the tests were carried out in the same manner except that the test was stopped at 25% strain. The sample was then recompressed to 25% strain and was allowed to relax for 30 min, at which time the sample length was measured. The

Table 1. Summary of Data for Epoxy Cross-Linked Aerogels from Optimization Study

run	total Si (mol/L)	APTES Si (mol %)	BTMSH Si (mol %)	BPGE to APTES	density (g/cm^3)	porosity (%)	shrinkage (%)	modulus (MPa)	recovered strain (%)	surface area (m^2/g)
1	1	30	20	0.7	0.360	72.7	25	56.1	3.9	b
2	1.6	15	0	0.5	0.365	75.2	22	82.0	3.1	342
3	1.6	15	0	0.7	0.248	85.4	11	18.2	2.2	322
4	1.6	15	40	0.5	0.278	82.1	13	23.2	1.2	329
5	1	30	20	0.6	0.315	80.0	22	37.8	3.4	b
6	1	30	40	0.6	0.310	77.6	20	42.4	3.7	103
7	1	30	20	0.5	0.269	79.5	20	32.7	2.6	219
8	1	30	20	0.6	0.300	77.3	21	40.7	a	b
9	1	30	0	0.6	0.346	76.7	24	b	b	206
10	1	30	20	0.6	0.274	79.4	19	30.1	3.3	186
11	1	15	20	0.6	0.198	85.9	18	12.7	2.4	392
12	1.6	15	40	0.7	0.284	81.2	12	23.1	1.3	303
13	1	30	20	0.6	0.307	76.6	23	33.9	3.4	b
14	1.6	45	0	0.7	0.670	52.9	19	260.1	6.7	97
15	1.6	30	20	0.6	0.533	60.2	22	150.6	4	139
16	1.6	45	40	0.5	0.847	35.9	28	326.6	a	36

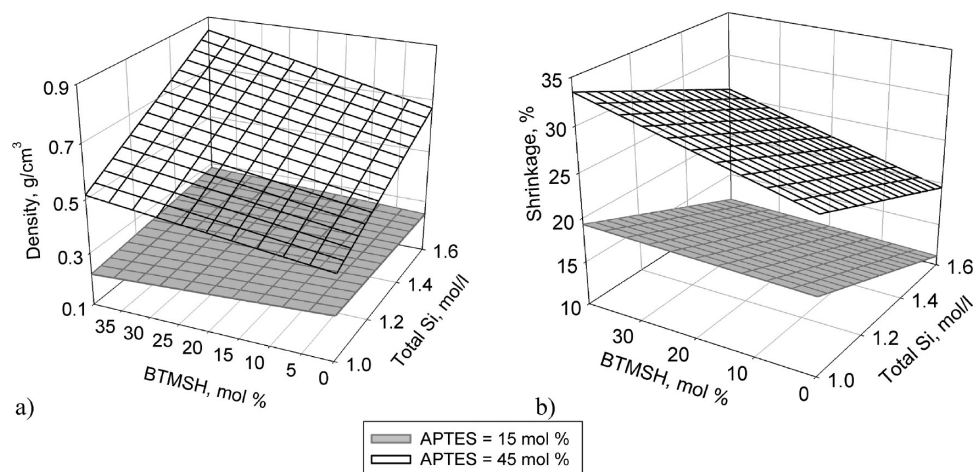^{a} Sample broke before 25% strain. ^{b} Not measured.

FIGURE 1. Graphs of empirical models of data from Table 1 for (a) density and (b) shrinkage vs total silicon concentration and mol fraction BTMSH.

amount of recovered strain is reported as the percent sample length recovered after the first compression. The amount of recovered strain measured after the second compression had greater random error and hence it was not used in the statistical modeling.

Statistical Modeling. Design Expert 7.1 from Stat-Ease, Inc., was used for statistical experimental design and analysis of the data. To reduce the number of experiments and allow computation of empirical models relating the variables to measured properties, a d-optimal design strategy was employed in the study. In all, 16 aerogel formulations were fabricated, including 4 repeats to assess model reliability and accuracy. The data were analyzed using multiple linear least-squares regression. All continuous, independent variables were orthogonalized (transformed to −1 to 1 range) before modeling. A full quadratic model was considered for each measured property, and terms deemed not statistically significant (<90% confidence) were removed from the model one at a time.

DISCUSSION

Preparation conditions and resulting properties of monoliths made in the study are shown in Table 1. Variables used in the study include the total concentration of silicon used

to prepare the gels, mol fraction of the total silicon derived from APTES and BTMSH (noting that BTMSH contributes two silicon atoms for every molecule, and the rest of the silicon is derived from TEOS), and the amount of epoxy (BPGE) in the sol given as a mole ratio to APTES. It is assumed that one epoxy molecule will react with two APTES amines. Hence, a BPGE to APTES ratio of 0.5 is stoichiometric, whereas a ratio 0.6−0.7 represents an excess of epoxy. By including the epoxy monomers in the initial sol, the synthesis is not only shortened but, because of the fact that cross-linking is not dependent on diffusion, polymer reinforcement is more efficient and more uniform. This is evidenced by the bulk densities of the monoliths made in the study, which ranged from 0.2 to up to 0.885 g/cm^3. Shown in Figure 1a is a graph of the empirical model for density (standard error = 0.019 g/cm^3, R^2 = 0.99+) derived from the measured monoliths. As seen in this graph, densities are much higher for aerogels made with higher concentrations of APTES. For aerogels made using 15 mol % APTES,
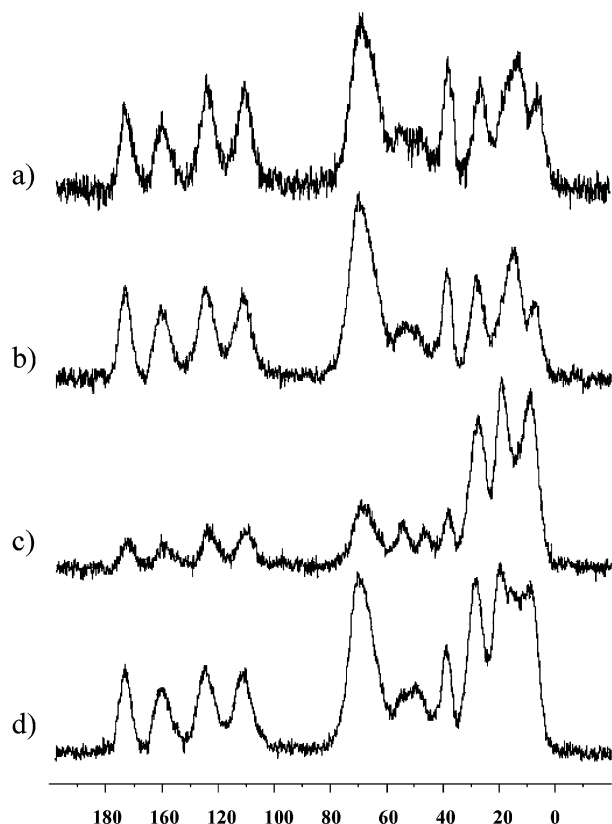
FIGURE 2. Solid ^{29}Si NMR of monoliths from runs listed, including (a) run 3 made from 15 mol % APTES Si and no BTMSH; (b) run 14 made from 45 mol % APTES Si and no BTMSH; (c) run 12 made from 15 mol % APTES Si and 40 mol % BTMSH Si; and (d) run 16 made from 45 mol % APTES Si and 40 mol % BTMSH Si.

FIGURE 3. Graph of the empirical model for porosity plotted vs fraction of Si derived from BTMSH and total silicon concentration.

densities are comparable to those previously made using a multistep synthesis, while the monoliths derived from 45 mol % APTES are 2−3 times more dense than previously reported (10). In fact, in earlier studies of aerogels made using APTES as an amine cross-linking site, increasing APTES was seen to increase density much less than expected (10) or to level off after a certain concentration (9), presumably because of surface saturation effects. That is, after a certain concentration of APTES, the surface of the secondary particles is completely covered with amine. Any further increase in APTES concentration results in amines inaccessible to the monomer diffusing into the gel because they are buried inside the secondary particles. Using a one-pot reaction scheme with the monomer already present in the gel as it is formed, all of the amines are accessible to monomer. As seen in the plot of the empirical model for shrinkage (standard error = 1.6 %, R^2 = 0.94) shown in Figure 1b, aerogels made using the one-pot method described herein using 15 mol % APTES tended to shrink less than monoliths made using 45 mol % APTES. However, this difference in shrinkage (10−15 %) is not enough to account for the dramatic increase in density.

As expected, density also increases with increasing total silicon and mol fraction of BTMSH concentration as seen in Figure 1a, because of greater amounts of silica and hexyl links in the resulting aerogels. Increasing the ratio of epoxy to APTES (not shown) has only a small effect on density,
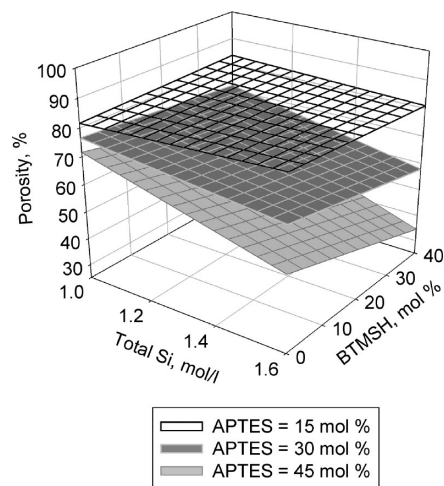
though using 0.5 equiv. of epoxy/APTES tended to result in more shrinkage of the monoliths. Thus, changes in properties which depend on density using lower equiv. of epoxy per APTES are more a result of shrinkage than an increase in polymer cross-linking. For this reason, all properties discussed and all graphs are shown with ratio of 0.7 epoxy molecules to APTES.

Solid ^{13}C CP-MAS NMR spectra of aerogels from the study are shown in Figure 2a-d. In all spectra, peaks in the aromatic region and the peak at 70 ppm are due to epoxy links. Peaks at 9−20 ppm are due to the propyl groups from APTES (and the hexyl links from BTMSH if present). The peak at approximately 30 ppm arises from the methyls on the isopropylidene group of the epoxy (and the middle methylenes from BTMSH, if present). Peaks at 40 and 50−60 ppm are due to the carbons next to nitrogen from the propyl group of APTES and the reacted epoxy links, respectively. As shown in Figure 2a (15 mol % APTES) and 2b (45 mol % APTES), spectra from monoliths made using no BTMSH are nearly identical, indicating that the degree of reaction between epoxy and propyl amine are about the same. This is in agreement with the large increase in density as the APTES fraction is increased—all of the amines are reacting even when using 45 mol % APTES. The spectrum shown in Figure 2c is from a monolith prepared using 15 mol % APTES and 40 mol % BTMSH. The epoxy peaks appear much smaller because of the increase in aliphatic peaks arising from BTMSH. However, the peak at 40 ppm (methylene of APTES next to nitrogen) is also much smaller and in line with the relative intensity of the epoxy peaks, again indicating that reaction of epoxy with amine is not affected by the presence of BTMSH. For the monolith prepared using 45 mol % APTES and 40 mol % BTMSH, the peaks due to epoxy and the 40 ppm peak due to methylene from APTES again grow larger, but remain about the same size relative to each other.

A response surface plot of porosity (standard error = 1.6 %, R^2 = 0.99), calculated from the bulk density and skeletal density measured by helium pycnometry, graphed
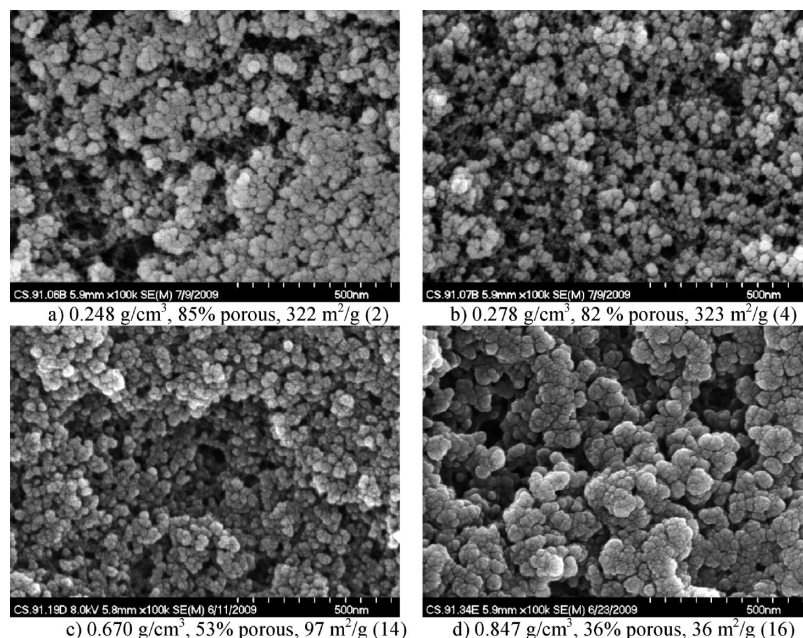
FIGURE 4. Side-by-side comparisons of micrographs of samples from Table 1 with (left) no BTMSH and (right) 40 mol % BTMSH-derived Si, including samples prepared (a, b) with 15 mol % APTES and (c, d) with 45 mol % APTES. All samples were prepared using 1.6 mol/L total silicon concentration. Sample numbers are shown in parentheses.

vs total silicon concentration and BTMSH fraction, is shown in Figure 3. Note that porosity decreases slightly because of increasing total silicon and BTMSH mol fraction, and dramatically decreases because of an increase in APTES concentration. Because porosity is a feature of aerogels important to their application, maintaining high levels of porosity is critical. Only monoliths made using APTES concentration of 15 mol % have porosities in excess of 80 %. Except at the lowest total Si concentration studied (1 mol/L), higher concentrations of APTES in a one-pot reaction scheme result in porosities too low for use in typical aerogel applications.

Scanning electron micrographs of representative monoliths made using 1.6 mol/L total silicon concentration are shown in Figure 4. Monoliths shown in Figure 4a (no BTMSH) and 4b (40 mol % BTMSH) made using 15 mol % APTES are similar in appearance to those previously reported using a multistep diffusion process (10). Note that the particle sizes are quite uniform in appearance in both micrographs, whereas the pores appear larger in Figure 4b, as previously observed for hexyl-linked monoliths. The monoliths are somewhat similar in density and porosity to those previously prepared using the multistep process. In contrast, monoliths shown in Figure 4c (no BTMSH) and 4d (40 mL % BTMSH) made with 45 mol % APTES are twice as dense and 20−30 % less porous than the same formulations made using a multistep process, again because of the near-complete reaction between APTES amines and epoxy obtained when diffusion is not a factor.

Mean pore diameter and surface area measurements were derived from nitrogen sorption data for all the samples using the Brunauer−Emmett−Teller (BET) method. Surface areas are listed in Table 1 and under micrographs shown in Figure 4. The pore size measured by nitrogen sorption is known to be underestimated for aerogels because of con-

traction of the structure (12). Nevertheless, observed trends are consistent with that seen by SEM. Graphs of pore volume vs pore diameter in Figure 5a illustrate a comparison of the same monoliths shown in the micrographs in Figure 4 which were made using 1.6 mol/L total silicon concentration. Note that the narrowest pore size distribution and smallest pores are obtained for monoliths made using 15 mol % APTES and no BTMSH. Increasing APTES and BTMSH broadens the pore distributions and also causes a shift to larger pore sizes as seen previously with monoliths made using a multistep process (10). Similar results are seen with lower total silicon concentrations. BET surface areas are also much reduced by increasing APTES concentration as seen in Figure 5b. Figure 5b shows empirical models for surface area (standard error $= 0.01$ $R^2 = 0.99+$) graphed vs total silicon concentration and BTMSH fraction. As can be seen in the plot, only 15 mol % APTES derived monoliths have surface areas higher than 300 m^2/g. Decreasing total silicon concentration and increasing BTMSH fraction also causes a small though significant decrease in surface area. In addition, as seen before with density and porosity, surface areas obtained for monoliths in this study prepared using 15 mol % APTES are comparable to the same formulations obtained from the multistep diffusion process, whereas for those prepared with 45 mol % APTES, the surface areas are reduced by a factor of 2.

The monoliths were also characterized using compression testing. Young's modulus taken from the initial slope of the stress−strain curves was modeled using multiple linear regression analysis. Graphs of the empirical model for modulus (standard error $=0.2$, $R^2 = 0.98$) vs total silicon concentration and BTMSH fraction are shown in Figure 6 for aerogels made using (a) 15 mol % APTES and (b) 45 mol % APTES. Increasing total silicon concentration and BTMSH fraction both significantly increase modulus as expected due
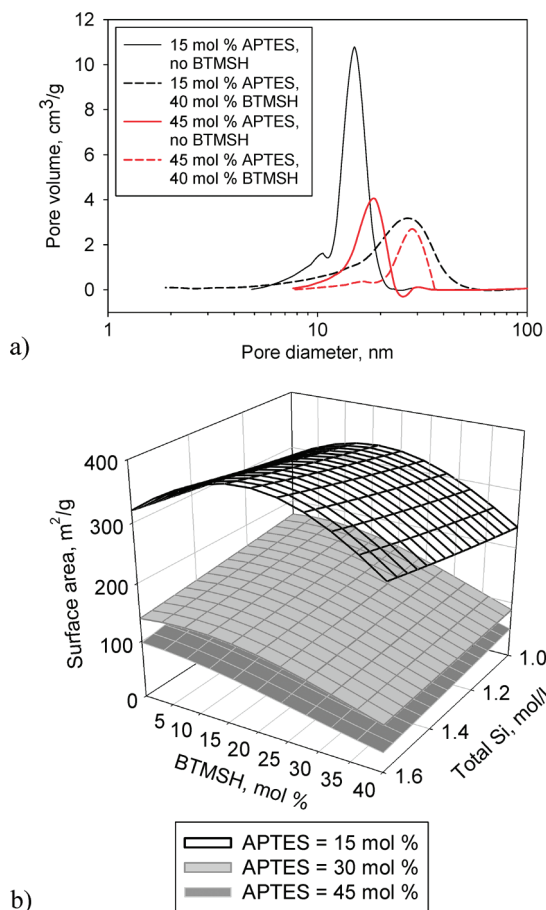
a)

b)

FIGURE 5. Graph of the (a) pore volume vs pore diameter of representative samples and (b) the empirical model for surface area plotted vs total Si concentration and mol fraction of Si derived from BTMS.

to small increases in density. It is interesting to note that modulus of monoliths prepared using the multistep diffusion method in the previous study did not increase with increasing BTMSH mol fraction (10). This was due to the fact that in the previous study, use of BTMSH was seen to reduce shrinkage, especially for lower APTES formulations, resulting in lower densities. Using a one-pot reaction scheme, shrinkage is more dependent on the amount of APTES and the

ratio of epoxy to APTES used. In the graphs shown in Figure 6, APTES mol fraction and epoxy to APTES ratios are held constant, making shrinkage a nonfactor in these plots. As seen in Figure 6b, monoliths made from 45 mol % APTES are an order of magnitude stronger because of the dramatic increase in density. However, as previously discussed, except for monoliths made using the lowest total Si concentration, these monoliths have extremely low porosity and surface area, reducing their utility as insulators or other applications usually considered for aerogels.

Elastic recovery after compression was also assessed by compressing samples to 25 % strain, followed by allowing them to relax. Typical stress strain curves for repeat compression tests are shown in Figure 7a for monoliths from Table 1 made using 1.6 mol/L total silicon and 15 % APTES. The solid black curves are the first and second compression for run 3 (no BTMSH) and the dashed red curves are for run 12 (40 mol % BTMSH). Interestingly, most of the samples made from the one-pot reaction scheme recover better than those made with the multistep diffusion process previously reported. In the examples shown, the sample containing no hexyl links recovered all but 2.2 % of the 25 % compared to 5 % for the multistep sample reported previously (10). Clearly, epoxy is contributing more to elastic recovery when included in the initial sol in the one pot reaction scheme. This may be due to the presence of epoxy inside of the secondary particles, whereas these smallest pores may not be accessible to epoxy in the diffusion controlled process. The sample with hexyl links recovered all but 1.3 % of the 25 %, which was similar to the multistep sample previously reported (all but 1 % unrecovered strain). Note, however, that modulus is slightly higher for the hexyl linked samples made using the one-pot reaction, again because of the slight increase in density.

CONCLUSIONS

Streamlining the process of making epoxy reinforced aerogels by eliminating the diffusion step produces aerogels of similar density and pore structure to those previously reported using a multistep reaction scheme when using 15 mol % APTES as amine cross-linking site. The process is
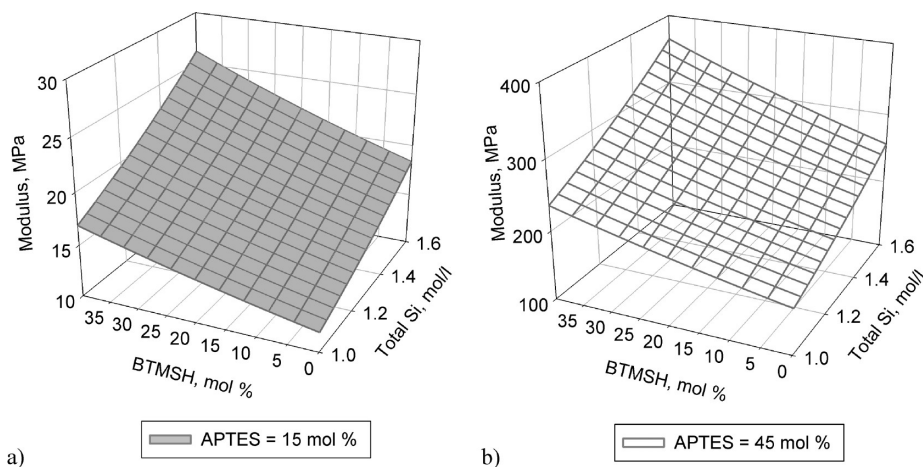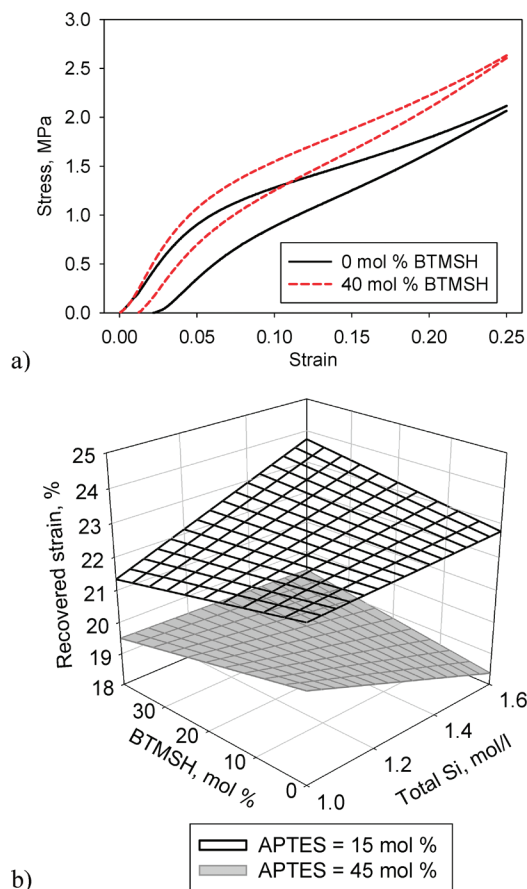

a)

b)

FIGURE 6. Empirical model of modulus from compression graphed vs total Si concentration and fraction of BTMSH-derived Si for (a) 15 mol % APTES and (b) 45 mol % APTES.

a)

b)

FIGURE 7. (a) Stress−strain curves for repeat compression tests taken to 25% strain where the solid lines are the first and second compression for sample containing no BTMSH and the dotted lines are the first and second compressions for the same formulation with 40 mol % BTSMH; and (b) graphs of empirical models for recovered strain after compression to 25% strain graphed vs total Si concentration and fraction of BTMSH-derived Si.

analogous to one recently used to fabricate PAN reinforced aerogels. However, by comparing aerogels fabricated from higher APTES concentrations made using both methods, we also present evidence for the first time that monomer is not diffused uniformly in gels using the multistep process. Aerogels made using a one-pot reaction scheme and high concentrations of APTES are extremely high in density with low percent porosities and extremely low surface areas compared to multistep aerogels. This is due to the complete reaction of epoxy with all amines present when diffusion into the gel is not a factor. In fact, using the one-pot method, only monoliths made using 15 mol % APTES can truly be considered aerogels and suitable for use as insulation or other applications requiring high surface areas, high porosity, and small pore sizes.

Slight improvements to mechanical properties over aerogels made using a multistep diffusion process are also evidenced. In particular, hexyl-linked aerogels made using

1.6 mol/L and 15 mol % APTES are similar in elastic recovery, density, and surface area to those previously reported using a multistep process, whereas the modulus is increased by a factor of 2. Most importantly, the method of making the aerogels is greatly simplified by eliminating two wash steps before cross-linking and the epoxy diffusion step. This reduces the amount of solvent needed to make the aerogels by at least half with no compromise in properties.

REFERENCES AND NOTES

(1) (a) Pierre, A. C.; Pajonk, G. M. *Chem. Rev.* **2002**, *102*, 4243–4265. (b) Morris, C. A.; Anderson, M. L.; Stroud, R. M.; Merzbacher, C. I.; Rolison, D. R. *Science* **1999**, *284*, 622–624. Pajonk, G. M. *Catal. Today* **1999**, *52*, 3–13.

(2) Essex Corporation, *Final Report on Advanced Extravehicular Activity Systems Requirements Definition Study*, **1989,** NAS9−17779.

(3) Paul, H. L.; Diller, K. R. *J. Biomechanical Engineering* **2003**, *125*, 639–647.

(4) Tang, H. H.; Orndoff, E. S.; Trevino, L. A. *36th International Conference on Environment Systems*, July 17−20, 2006, Norfolk, Virginia AIAA 2006−01−2235.

(5) (a) Zhang, G.; Dass, A.; Rawashdeh, A.-M. M.; Thomas, J.; Counsil, J. A.; Sotiriou-Leventis, C.; Fabrizio, E. F.; Ilhan, F.; Vassilaras, P.; Scheiman, D. A.; McCorkle, L.; Palczer, A.; Johnston, J. C.; Meador, M. A. B.; Leventis, N. *J. Non-Cryst. Solids* **2004**, *350*, 152–164. (b) Leventis, N.; Sotiriou-Leventis, C.; Zhang, G.; Rawashdeh, A.-M. M. *Nano Lett.* **2002**, *2*, 957–960.

(6) Meador, M. A. B.; Capadona, L. A.; McCorkle, L.; Papadopoulos, D. S.; Leventis, N. *Chem. Mater.* **2007**, *19*, 2247–2260.

(7) Boday, D. J.; Stover, R. J.; Muriithi, B.; Keller, M. W.; Wertz, J. T.; Obrey, K. A. D.; Loy, D. A. *ACS Applied Mater. and Interfaces* **2009**, *1*, 1364–1369. (2009) Strong, Low-Density Nanocomposites by Chemical Vapor Deposition and Polymerization of Cyanoacrylates on Aminated Silica Aerogels.

(8) (a) Ilhan, U. F.; Fabrizio, E. F.; McCorkle, L.; Scheiman, D. A.; Dass, A.; Palczer, A.; Meador, M. A. B.; Johnston, J. C.; Leventis, N. *J. Mater. Chem.* **2006**, *16*, 3046–3054. (b) Mulik, S.; Sotiriou-Leventis, C.; Churu, G.; Lu, H.; Leventis, N. *Chem. Mater.* **2008**, *20* (15), 5035–5046. (c) Baochau N., Nguyen; Mary Ann, B. Meador; Marissa E., Tousley; Brian, Shonkwiler *Polym. Prepr.* **2008**, *49* (1), 340. Nguyen, B. N.; Meador, M. A. B.; Tousley, M. E.; Shonkwiler, B.; McCorkle, L.; Scheiman, D. A.; Palczer, A. *ACS Applied Mater. and Interfaces* **2009**, *1*, 621–630.

(9) Meador, M. A. B.; Fabrizio, E. F.; Ilhan, F.; Dass, A.; Zhang, G.; Vassilaras, P.; Johnston, J. C.; Leventis, N. *Chem. Mater.* **2005**, *17*, 1085–1098.

(10) Meador, M. A. B.; Weber, A.; Hindi, A.; Naumenko, M.; McCorkle, L.; Quade, D.; Vivod, S. L.; Gould, G. L.; White, S.; Deshpande, K. *ACS Appl. Mater. Interfaces* **2009**, *1*, 894–906.

(11) Leventis, N.; Sadekar, A.; Chandrasekaran, N.; Sotiriou-Leventis, C. *Chem. Mater.* **2010**, *22*, 2790–2803.

(12) Scherer, G. W.; Smith, D. M.; Stein, D. *J. Non-Cryst. Solids* **1995**, *186*, 309–315.

AM100422X